Journal of Simulation and Analysis of Novel Technologies in Mechanical Engineering
16 (3) (2024) 0061~0077
DOI 10.71939/jsme.2024.1190493

Research Article

Nonlinear radial vibration of single-walled carbon nanotubes using numerical methods

Zahra Azimzadeh[1] , Alireza Fatahi-Vajari[2,*]

[1]*Department of Mathematics, YI.C., Islamic Azad University, Tehran, Iran*
[2]*Department of Mechanical Engineering, Shahr.C., Islamic Azad University, Shahriar, Iran*

[*] afatahiv@iau.ac.ir

(Manuscript Received --- 14 Nov. 2024; Revised --- 27 Jan. 2025; Accepted --- 25 Feb. 20245)

Abstract

This paper investigates the nonlinear radial breathing mode (RBM) vibration of single-walled carbon nanotubes (SWCNTs) based on numerical methods. A second order partial differential equation that governs the nonlinear RBM vibration for such nanotubes is derived using doublet mechanics (DM). This nonlinear equation is reduced to ordinary differential equation using Galerkin method and then solved using Homotopy perturbation method (HPM) to obtain the nonlinear natural frequency in nonlinear RBM vibration. It is the first time that DM is used to model the nonlinear RBM vibration of CNTs. It is shown that tube radius and the amplitude of vibration play significant role in the nonlinear RBM vibration response of SWCNTs. Increasing the vibration amplitude decreases the natural frequency of vibration compare to the predictions of the linear models. However, with increase in tube radius, the effect of vibration amplitude on the natural frequency decreases. To show the accuracy and capability of this method, the results obtained herein are compared with the numerical results and good agreement is observed. It is notable that the results generated herein are new and can be served as a benchmark for future works.

Keywords: doublet mechanics, homotopy perturbation method, radial breathing mode vibration, single-walled carbon nanotubes, nonlinear vibration.

1- Introduction

At nanoscale levels, the mechanical characteristics of nanostructures are often significantly different from their behavior at macroscopic scale due to the inherent size effects. Such characteristics greatly affect the performance of nanoscale materials or structures and nanoinstruments. In addition to mechanical properties, size effects can influence electronic, optical and other properties [1]. Classical continuum mechanics modeling assumptions are conducive to erroneous results, when applied to material domains where the typical microstructural dimension is comparable

with the structural ones [2]. Currently, various elegant modifications to continuum mechanics have been proposed to incorporate scale and microstructural features into the theory. These theories are introduced as generalized continuum mechanics [3- 7]. For example, Oveissi et al. analytically determined the nonlocal parameter to obtain one more accurate axial-buckling response of carbon nanoshells conveying nanofluids using four plates/shells' classical theories incorporating Eringen's nonlocal theory [7]. One particular theory that has recently been applied to materials with microstructure is doublet mechanics (DM). This theory originally developed by Granik (1978), has been applied to granular materials by Granik and Ferrari (1993) [2] and Ferrari et al. (1997) [8]. In DM micromechanical models, solids are represented as arrays of points, particles or nodes at finite distances. This theory has shown good promise in predicting observed behaviors that are not predictable using continuum mechanics. Such behaviors include the so-called Flamant paradox [8]. Some applications of DM has been given in [9- 17].

Single-walled carbon nanotubes (SWCNTs) are tiny cylinders made from carbon. A SWCNT can be described as a single layer of a graphite crystal that is rolled up into a seamless circular cylinder, one atom thickness, usually with a small number of carbon atoms along the circumference and a long length along the cylinder axis. SWCNTs have many unique, fascinating properties. They are very strong and have extremely light weight. They are excellent conductors of heat, and transport electrons easily. Because of these special properties, they might be used as the substantial parts of nanoelectronics, nanodevices, and nanocomposites. The properties of CNTs depend strongly on their microscopic structure [18]. Then, in recent years, considerable effort has been devoted to the problem of the vibration of these nanomaterials. One of the most modes of vibration for SWCNTs is radial breathing mode (RBM) vibration. This mode is the first and main mode in radial vibration of tubes. In fundamental studies, it is desired to know which nanotube is probed experimentally. The growth of CNTs with a predefined microscopic structure remains a major challenge. In principle, the chiral index of an individual tube can be determined by optical spectroscopy like photoluminescence and Raman scattering. However, the experimental error in the measurement of diameter and chiral angle leads to uncertainties in the assignment of the chiral index [18]. The RBM is the characteristic phonon mode of SWCNTs which leads to a periodic increase and decrease of the tube diameter [18]. In the RBM, all carbon atoms move coherently in the radial direction creating a breathing-like vibration of the entire tube [18, 19]. This feature is specific to CNTs and is not observed in other carbon systems such as graphite [19]. The RBM frequency is usually the strongest feature in SWCNT Raman spectra which plays a crucial role in the experimental determination of the geometrical properties of SWCNTs [19, 20]. RBM frequencies are very useful for identifying a given material containing SWCNTs, through the existence of RBM modes, and for characterizing the nanotube diameter distribution in the sample through

inverse proportionality of the RBM frequency to the tube diameter [20, 21]. Therefore, it is very important to know the behavior of RBM frequency of different nanotubes, precisely.

However, most of the investigations conducted on the RBM vibration of CNTs have been restricted to the linear theory. As the best knowledge of the authors, the nonlinear radial vibration of nanotube is not investigated and the present paper tries to consider such effect. On the other hands, nonlinearity may affect the results, and then it is important to investigate the nonlinear RBM vibration. The HPM as a powerful analytical approach was first introduced by He [22- 32] for solving various linear and nonlinear initial and boundary value problems. The HPM in applied mathematics is widely studied now by most mathematicians. In this method, the solution is considered as the sum of an infinite series which converges rapidly to the exact solution. Usually, one or two iterations lead to high accuracy of the solution. The series used is a series of functions rather than terms as is in Taylor series. The method has recently been applied to a wide class of differential and integral equations, stochastic and deterministic problems, linear and non-linear equations. The advantages of this method to other methods is more simplicity, give better results and with time saving because in this method convergence is especially rapid in the non-linear and nonhomogeneous equations [33]. The HPM was also studied by many mathematicians and engineers to investigate nonlinear equations arising in science and engineering. This simple method has been applied to solve linear and nonlinear equations in different fields of mechanics like heat transfer, fluid mechanics and so on [34- 42].

Nonlinear RBM vibration analysis of nanotubes based on DM has not yet been investigated analytically and the present work attempts to consider such analysis. The present work is an extension of the authors' previous work for free linear RBM vibration of SWCNTs with free boundary conditions [9]. The main idea of the paper is to obtain the nonlinear RBM frequency of vibration of SWCNTs which incorporates explicitly vibration amplitude and scale effects using HPM. First, after a brief review of nonlinear DM, doublet mechanical theory is applied to obtain the basic equations of motion for nonlinear RBM vibration of SWCNTs. Then, HPM is applied to solve the nonlinear governing equations to obtain the nonlinear frequency equation for nonlinear RBM vibration mode of SWCNTs. Another aim of this investigation is to show the effectiveness of HPM and the capability of this simple method and also handling the nonlinear RBM for obtaining the nonlinear natural frequency in RBM of SWCNTs. It is shown that the first approximate solution of New HPM admits a remarkable accuracy in comparison with the results obtained from the numerical method for the amplitude-frequency curves.

2- Nonlinear equation of motion in DM

DM is a micromechanical theory based on a discrete material model whereby solids are represented as arrays of points or nodes at finite distances. A pair of such nodes is referred to as a doublet, and the nodal spacing distances introduce length scales into the microstructural theory. Each node in the

array is allowed to have a translation and rotation, and increments of these variables are expanded in a Taylor series about the nodal point. The order at which the series is truncated defines the degree of approximation employed. The lowest order case using only a single term in the series will not contain any length scales, while using more than one term will produce a multi length scale theory. This allowable kinematics develops microstrains of elongation, shear and torsion (about the doublet axis). Through appropriate constitutive assumptions, these microstrains can be related to corresponding elongational, shear and torsional microstresses. Applications of this theory to geomechanics problems have been given by Granik and Ferrari (1993) [2] and Ferrari et al. (1997) [8]. For these applications, a granular interpretation of DM has been employed, in which the material is viewed as an assembly of circular or spherical particles. A pair of such particles represents a doublet as shown in Fig. 1.

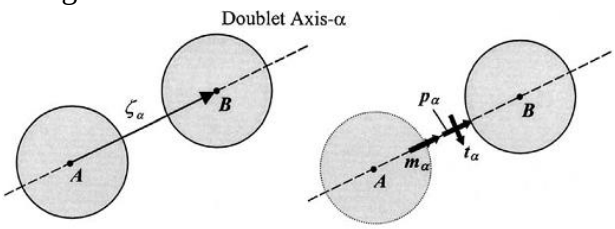

Fig. 1 doublet

Corresponding to the doublet *(A, B)* there exists a doublet or branch vector $\boldsymbol{\zeta}_a$ connecting the adjacent particle centers and defining the doublet axis. The magnitude of this vector $\eta_a = |\boldsymbol{\zeta}_a|$ is simply the particle diameter for particles in contact. However, in general the particles need not be in contact, and for this case the length scale η_a could be used to represent a more general microstructural feature. For example, the internal characteristic scale for the crystal lattice parameter of carbon is $\eta_a = 1.421\ a$ [13].

As mentioned, the kinematics allow relative elongational, shearing and torsional motions between the particles, and this is used to develop an elongational microstress p_a, shear microstresst_a, and torsional microstress m_a as shown in Fig. 1. It should be pointed out that these microstresses are not second order tensors in the usual continuum mechanics sense. Rather, they are vector quantities that represent the elastic microforces and microcouples of interaction between doublet particles. Their directions are dependent on the doublet axes which are determined by the material microstructure. These microstresses are not continuously distributed but rather exist only at particular points in the medium being simulated by DM.

From Fig. 2, suppose doublet (a, b_α) transform to doublet ($\acute{a}, \acute{b}_\alpha$) as a result of kinematic translation. The superscript *0* for vectors indicates the initial configuration.

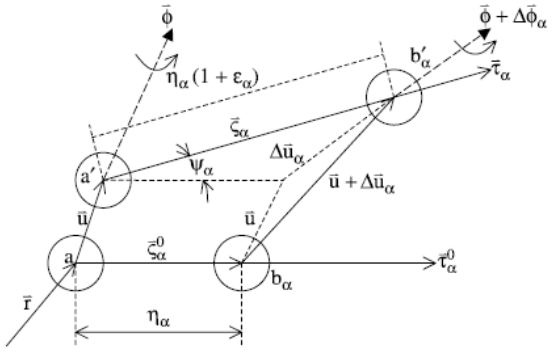

Fig. 2 Translations of the doublet nodes $a \in A$, $b_\alpha \in B_\alpha$

If $\boldsymbol{u}(\boldsymbol{x},t)$ is the displacement field coinciding with a particle displacement, then the incremental displacement is written as:

$$\Delta \boldsymbol{u}_\alpha = \boldsymbol{u}(\boldsymbol{x}+\boldsymbol{\zeta}_\alpha^0, t) - \boldsymbol{u}(\boldsymbol{x},t) \tag{1}$$

where $\boldsymbol{x}$ is the position vector of paricle.

The incremental function in (1) could be expanded in a Taylor series as [8]:

$$\Delta \boldsymbol{u}_\alpha = \sum_{\chi=1}^{M} \frac{(\eta_\alpha)^\chi}{\chi!} (\boldsymbol{\tau}_\alpha^0 . \boldsymbol{\nabla})^\chi \boldsymbol{u} \tag{2}$$

Where in $\boldsymbol{\nabla}$ is the Del operator in general coordinates and η is the internal characteristic length scale. As mentioned above, the number of terms used in the series expansion of the local deformation field determines the order of the approximation in DM.

Here, $\alpha = 1,\ldots,n$ while n is referred to the numbers of doublets. For the problem under study, it is assumed that the shear and torsional micro-deformations and micro-stresses are negligible and thus only extensional strains and stresses exist.

The extensional micro-strain scalar measure ϵ_α, representing the axial deformation of the doublet vector, is defined as [8]:

$$\epsilon_\alpha = \frac{\boldsymbol{\tau}_\alpha . \Delta \boldsymbol{u}_\alpha}{\eta_\alpha} \tag{3}$$

From Fig. 1, it can be written that

$$\boldsymbol{\tau}_\alpha = \frac{1}{1+\epsilon_\alpha}\left(\boldsymbol{\tau}_\alpha^0 + \frac{\Delta \boldsymbol{u}_\alpha}{\eta_\alpha}\right) \tag{4}$$

As in linear elasticity, it is assumed that the relative displacement $|\Delta \boldsymbol{u}_\alpha|$ is small compared to the doublet separation distance η_α ($|\Delta \boldsymbol{u}_\alpha| \ll \eta_\alpha$) so that it may be assumed that $\boldsymbol{\tau}_\alpha = \boldsymbol{\tau}_\alpha^0$.

Now, the nonlinear basis of DM in radial vibration is expanded with more details. In nonlinear elasticity $\boldsymbol{\tau}_\alpha \neq \boldsymbol{\tau}_\alpha^0$ and the following approximate relations between $\boldsymbol{\tau}_\alpha$ and $\boldsymbol{\tau}_\alpha^0$ are present

$$\boldsymbol{\tau}_\alpha . \boldsymbol{\tau}_\alpha^0 = \cos(\psi_\alpha) = 1 - \frac{\psi_\alpha^2}{2} \tag{5}$$

$$\boldsymbol{\tau}_\alpha \times \boldsymbol{\tau}_\alpha^0 = \sin(\boldsymbol{\psi}_\alpha) = \boldsymbol{\psi}_\alpha \tag{6}$$

wherein ψ_α is the angle between initial and current branch vectors.

From (4)- (6), ψ_α^2 can be obtained as follow

$$\psi_\alpha^2 = \frac{1}{\eta_\alpha^2\left(1+2\epsilon_\alpha+\epsilon_\alpha^2\right)}\left(\Delta \boldsymbol{u}_\alpha \times \boldsymbol{\tau}_\alpha^0\right).\left(\Delta \boldsymbol{u}_\alpha \times \boldsymbol{\tau}_\alpha^0\right) \tag{7}$$

If ψ_α^2 obtained from (7) is substituted in (3), it can be concluded that

$$\frac{(\Delta \boldsymbol{u}_\alpha \times \boldsymbol{\tau}_\alpha^0).(\Delta \boldsymbol{u}_\alpha \times \boldsymbol{\tau}_\alpha^0)}{\eta_\alpha^2(1+2\epsilon_\alpha+\epsilon_\alpha^2)} = 2 - \frac{2}{1+\epsilon_\alpha}\left(1 + \frac{\Delta \boldsymbol{u}_\alpha . \boldsymbol{\tau}_\alpha^0}{\eta_\alpha}\right) \tag{8}$$

With solving this equation, the microstrain for nonlinear approximation can be obtained. It is clear that for linear approximation that $\Delta \boldsymbol{u}_\alpha \times \boldsymbol{\tau}_\alpha^0 = 0$ and then the linear approximation can be obtained. Multiplication both side of (8) with $\frac{1}{2}\left(1+2\epsilon_\alpha+\epsilon_\alpha^2\right)$ yields

$$\frac{1}{2\eta_\alpha^2}(\Delta \boldsymbol{u}_\alpha \times \boldsymbol{\tau}_\alpha^0).(\Delta \boldsymbol{u}_\alpha \times \boldsymbol{\tau}_\alpha^0) + (1+\epsilon_\alpha)\left(1 + \frac{\Delta \boldsymbol{u}_\alpha . \boldsymbol{\tau}_\alpha^0}{\eta_\alpha}\right) = 1 + 2\epsilon_\alpha + \epsilon_\alpha^2 \tag{9}$$

In Eq. (9), ignoring ϵ_α^2 in comparison with ϵ_α and $\epsilon_\alpha \frac{\Delta u_{\alpha i}\tau_{\alpha i}^0}{\eta_\alpha}$ in comparison with $\frac{\Delta u_{\alpha i}\tau_{\alpha i}^0}{\eta_\alpha}$, gives the following approximate nonlinear microstrain-displacements equation as

$$\epsilon_\alpha = \frac{\Delta \boldsymbol{u}_\alpha . \boldsymbol{\tau}_\alpha^0}{\eta_\alpha} + \frac{1}{2\eta_\alpha^2}\left(\Delta \boldsymbol{u}_\alpha \times \boldsymbol{\tau}_\alpha^0\right).\left(\Delta \boldsymbol{u}_\alpha \times \boldsymbol{\tau}_\alpha^0\right) \quad (10)$$

We may write $\boldsymbol{\tau}_\alpha^0 = \tau_{\alpha j}^0 \boldsymbol{e}_j$ where $\tau_{\alpha j}^0$ are the cosines of the angles between the directions of micro-stress and the coordinates and $\boldsymbol{e}_i$ is the unit vector in Cartesian coordinate. Setting $\boldsymbol{\tau}_\alpha^0 = \tau_{\alpha i}^0 \boldsymbol{e}_i$, $\Delta \boldsymbol{u}_\alpha = \Delta u_{\alpha i} \boldsymbol{e}_i$ in (10), it is concluded that

$$\epsilon_\alpha = \frac{1}{2\eta_\alpha^2}\left(\Delta u_{\alpha i}\Delta u_{\alpha i}\tau_{\alpha j}^0\tau_{\alpha j}^0 - \Delta u_{\alpha i}\Delta u_{\alpha j}\tau_{\alpha i}^0\tau_{\alpha j}^0\right) + \frac{\Delta u_{\alpha i}\tau_{\alpha i}^0}{\eta_\alpha} \quad (11)$$

In DM under such assumptions and neglecting temperature effect, the relation between microstrain and microstress is written in the below [8].

$$p_\alpha = \sum_{\beta=1}^{n} A_{\alpha\beta}\epsilon_\beta \quad (12)$$

Where in p_α is axial micro stress along doublet axes. An example of the axial micro-stress is the interatomic forces between atoms or molecules located at the nodes of a general array such as a crystalline lattice. In the case of linear and homogeneous inter nodal central interactions. (12) can be interpreted as the constitutive equation in the linear and homogeneous DM and $A_{\alpha\beta}$ is the matrix of the micromodules of the doublet.

In the homogeneous and isotropic media with local interaction the above relation is simplified as below [8]:

$$p_\alpha = A_0\epsilon_\alpha \quad (13)$$

The relation between microstresses and macrostresses is [8]:

$$\boldsymbol{\sigma}^{(M)} = \sum_{\alpha=1}^{n} \boldsymbol{\tau}_\alpha^0\boldsymbol{\tau}_\alpha^0 \sum_{\chi=1}^{M} \frac{(-\eta_\alpha)^{\chi-1}}{\chi!}(\boldsymbol{\tau}_\alpha^0.\boldsymbol{\nabla})^{\chi-1} p_\alpha \quad (14)$$

Substituting (11) into (13) and the result into (14) and neglecting scale effect yields

$$\sigma_{mn} = A_0\tau_{\alpha m}^0\tau_{\alpha n}^0\left[\frac{\Delta u_{\alpha i}.\tau_{\alpha i}^0}{\eta_\alpha} + \frac{1}{2\eta_\alpha^2}\left(\Delta u_{\alpha i}\Delta u_{\alpha i}\tau_{\alpha j}^0\tau_{\alpha j}^0 - \Delta u_{\alpha i}\Delta u_{\alpha j}\tau_{\alpha i}^0\tau_{\alpha j}^0\right)\right] \quad (15)$$

This equation is the relation between macrostresses and displacements in nonlinear regime.

The three dimensional equation of motion in DM is given by [8]:

$$\boldsymbol{\nabla}.\boldsymbol{\sigma}^{(M)} + F_i = \rho\frac{\partial^2 u_i}{\partial t^2} \quad (16)$$

where in ρ is the mass density, $\boldsymbol{u}$ is the displacement vector and t is the time. Superscript (M) refers to the generalized macro stresses which incorporate scale effects.

Now, the form of matrix $[\boldsymbol{A}]$ in (4) containing elastic macroconstant for plane problem (two-dimensional) is obtained. For this reason, consider Fig. 3. According to Fig. 3, in the $x_1 - x_2$ plane, there are only three doublets with equal angels between them. The solution for the scale-less condition can be calculated directly from the associated continuum mechanics problem for an isotropic material.

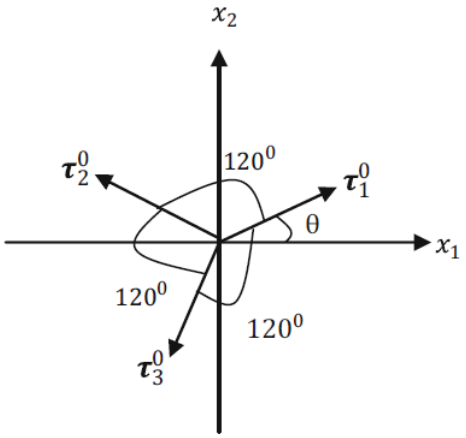

Fig. 3 Three doublets with equal angle 120^0 between them

Now the matrix A in (4) containing elastic macro constant in plane problem (two dimensional) is obtained. A plane problem with three doublets in the plane is considered under scale less conditions ($M = 1$), and the result obtained in DM is expected to coincide with the continuum mechanics result. For the plane problems in the homogeneous media, $[\boldsymbol{A}]$ is a symmetric matrix of order *3* with the most general form [8]

$$A = \begin{bmatrix} a & b & b \\ b & a & b \\ b & b & a \end{bmatrix} \tag{17}$$

According to Fig. 3, in the $x_1 - x_2$ plane there are only three doublets with equal angels between them. Then the solution can be calculated directly from the associated continuum mechanics problem in the scale less condition with an isotropic material.

It can be shown [16] that for any θ, if (17) is substituted into (12), and (16) for plane stress is used, the coefficients a and b in matrix A are found to be:

$$a = \frac{4}{9}\mu\frac{7\lambda+10\mu}{\lambda+2\mu}\ , b = \frac{4}{9}\mu\frac{\lambda-2\mu}{\lambda+2\mu} \tag{18}$$

Where $\lambda\ , \mu$ are Lame constants and can be written in term of elasticity modulus E, Poisson ratio ν and shear modulus G as below

$$\lambda = \frac{\nu E}{(1+\nu)(1-2\nu)}\ , \mu = G = \frac{E}{2(1+\nu)} \tag{19}$$

One could use $b = 0$as a quantitative guide to the applicability of the simpler constitutive relations such as (13). If $\lambda = 2\mu$ (or $\nu = \frac{1}{3}$) in plane stress condition from (18), it is concluded that $b = 0$ and

$$a = A_0 = \frac{8\mu}{3} = E \tag{20}$$

3- Modeling of nonlinear RBM vibration using DM

Specific applications of DM have been developed for two-dimensional problems with regular particle packing microstructures. In particular, the two-dimensional hexagonal packing microstructure without internal atoms establishes three doublet axes at 120^0 angles as shown in Fig. 3.

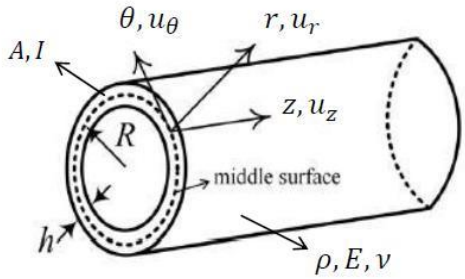

Fig. 4 A nanotube in cylindrical coordinate.

Now, consider a SWCNT of length L, mean radius R, Young's modulus E, Poisson's ratio ν and mass density ρ as shown in Fig. 4. Wherein u_r, u_θ and u_z are the displacements of the tube in radial, circumferential and axial directions in the cylindrical coordinates, respectively.

The equations of motion for SWCNTs In the cylindrical coordinates are as follow [9, 17]

$$\frac{\partial N_{zz}}{\partial z}+\frac{1}{r}\frac{\partial N_{\theta z}}{\partial \theta}+\rho f_z=\rho\frac{\partial^2 u_z}{\partial t^2} \quad (21)$$

$$\frac{\partial N_{z\theta}}{\partial z}+\frac{1}{r}\frac{\partial N_{\theta\theta}}{\partial \theta}+\frac{N_{\theta r}}{r}+\rho f_\theta=\rho\frac{\partial^2 u_\theta}{\partial t^2} \quad (22)$$

$$\frac{\partial N_{zr}}{\partial z}+\frac{1}{r}\frac{\partial N_{\theta r}}{\partial \theta}-\frac{N_{\theta\theta}}{r}+\rho f_r=\rho\frac{\partial^2 u_r}{\partial t^2} \quad (23)$$

$$\frac{\partial M_{zz}}{\partial z}+\frac{1}{r}\frac{\partial M_{\theta z}}{\partial \theta}+\rho\bar{l}_z=N_{zr} \quad (24)$$

$$\frac{\partial M_{z\theta}}{\partial z}+\frac{1}{r}\frac{\partial M_{\theta\theta}}{\partial \theta}+\frac{1}{r}M_{\theta r}+\rho\bar{l}_\theta=N_{\theta r} \quad (25)$$

$$\frac{M_{zr}}{\partial z}+\frac{1}{r}\frac{M_{\theta r}}{\partial \theta}-\frac{M_{\theta\theta}}{r}+\rho\bar{l}_r=N_{rr} \quad (26)$$

which are the equations of motion of a thin shell in the cylindrical coordinates.

Also, assuming that the shell-like body is thin, (27) and (28) may be used to write the physical components N_{ij} and M_{ij} as:

$$N_{ij}=\int_{-\frac{h}{2}}^{\frac{h}{2}}\sigma_{ij}^{(M)}dz\ ,i,j=1,2,3 \quad (27)$$

$$M_{ij}=\int_{-\frac{h}{2}}^{\frac{h}{2}}z\sigma_{ij}^{(M)}dz\ ,i,j=1,2,3 \quad (28)$$

Now, the equation of motion for nonlinear RBM is derived. To this end, the following assumptions, known as Love's first approximation, for cylindrical shells are made [9]:

1. All points that lie on a normal to the middle surface before deformation do the same after the deformation. Then the transverse shear stresses $\sigma_{rz}^{(M)}$ and $\sigma_{\theta z}^{(M)}$ are assumed to be negligible.
2. Displacements are small compared to the shell thickness.
3. The normal stresses in the thickness direction ($\sigma_{rr}^{(M)}$) are negligible (planar state of stress).

As mentioned before, in the RBM, all carbon atoms move coherently in the radial direction creating a breathing-like vibration of the entire tube. This feature is specific to CNTs and is not observed in other carbon systems such as graphite [20]. Therefore, RBM frequencies are very useful for identifying whether a given material contains CNTs, through the presence of RBM modes. The force needed for a radial deformation of a nanotube increases as the diameter (and hence the circumference) decreases [9]. Small nonradial component of the atomic displacement arises from mixing with the fully symmetric high-energy phonons. If the nanotube is approximated by a homogeneous cylinder, the frequency of the radial vibration is linear with the inverse tube diameter [18]. Thus, with assumptions of axisymmetric and homogeneity for the entire tube in the RBM

vibration, this implies that $\frac{\partial}{\partial \theta}=0, \frac{\partial}{\partial z}=0$ and $u_z=0, u_\theta=0$.

With the following assumptions in mind, from (11), the microstrains can be written in cylindrical coordinates as (see Appendix A):

$$\epsilon_\alpha=\frac{1}{r}\left(\tau_{\alpha\theta}^0\right)^2 u_r+\frac{1}{2r^2}\left(\tau_{\alpha\theta}^0\right)^2(\tau_{\alpha z}^0)^2 u_r^2 \quad (29)$$

It is further assumed that all doublets originating from a common node have the same magnitudes; i.e. $\eta_a=\eta\ (a=1,2,\ldots,n)$ and the interactions are purely axial (no shear or torsional microstresses is present). For local interaction in the plane, there will be two micromoduli a , b and the constitutive relationship between elongation microstress and microstrain is expressed by (4). If $\nu=\frac{1}{3}$, then matrix $[\boldsymbol{A}]$ will be diagonal and there will be one micromodulusA_0 and the constitutive relationship between elongation microstress and microstrain is expressed by (5). In this paper, (4) is used.

If (29) is substituted into (13) and the result into (14), the macrostress-displacement relations in the cylindrical coordinates may be written as:

$$\sigma_{ij}=\sum_{\alpha=1}^3 \tau_{\alpha i}^0 \tau_{\alpha j}^0 \sum_{\beta=1}^3 A_{\alpha\beta}\left[\frac{1}{r}\left(\tau_{\alpha\theta}^0\right)^2 u_r+\frac{1}{2r^2}\left(\tau_{\alpha\theta}^0\right)^2(\tau_{\alpha z}^0)^2 u_r^2\right] \quad (30)$$

This equation is the relation between the macrostresses and the displacements. Considering such assumptions and neglecting body forces, (21)- (26) reduce to

$$\frac{1}{R}N_{\theta\theta}=\rho h\frac{\partial^2 u_r}{\partial t^2} \quad (31)$$

Setting i and j equal to θ in (50), the following equation for the normal stress $\sigma_{\theta\theta}^{(M)}$ is found

$$\sigma_{\theta\theta}^{(M)}=\sum_{\alpha=1}^3\left(\tau_{\alpha\theta}^0\right)^2\sum_{\beta=1}^3 A_{\alpha\beta}\left[\frac{1}{r}\left(\tau_{\alpha\theta}^0\right)^2 u_r+\frac{1}{2r^2}\left(\tau_{\alpha\theta}^0\right)^2(\tau_{\alpha z}^0)^2 u_r^2\right] \quad (32)$$

If (51) is substituted into (38) and then integrated along the tube thickness, the following equation is obtained

$$N_{\theta\theta}=h\sum_{\alpha=1}^3\left(\tau_{\alpha\theta}^0\right)^2\sum_{\beta=1}^3 A_{\alpha\beta}\left[\frac{1}{r}\left(\tau_{\alpha\theta}^0\right)^2 u_r+\frac{1}{2r^2}\left(\tau_{\alpha\theta}^0\right)^2(\tau_{\alpha z}^0)^2 u_r^2\right] \quad (33)$$

Substituting (17) into (33) and taking note that the nanotube in RBM vibration can be considered to be in the state of plane stress, from (18), (33) can be simplified to

$$N_{\theta\theta}=\frac{E}{1-\nu^2}h\sum_{\alpha=1}^3\left[\frac{1}{R}\left(\tau_{\alpha\theta}^0\right)^4 u_r+\frac{1}{2R^2}\left(\tau_{\alpha\theta}^0\right)^4(\tau_{\alpha z}^0)^2 u_r^2\right] \quad (34)$$

Inserting (34) into (31), the following equation is obtained.

$$-\frac{1}{R}\frac{A_0}{1-\nu^2}h\sum_{\alpha=1}^3\left[\frac{1}{R}\left(\tau_{\alpha\theta}^0\right)^4 u_r+\frac{1}{2R^2}\left(\tau_{\alpha\theta}^0\right)^4(\tau_{\alpha z}^0)^2 u_r^2\right]=\rho h\frac{\partial^2 u_r}{\partial t^2} \quad (35)$$

According to (31) a second-order nonlinear governing equation is obtained. However, the governing equation derived from the DM principle turns out to be an infinite order differential equation in terms of η. Because it is almost impossible to solve the infinite order differential equation, only terms of

order and lower in the infinite series in (10) and (14) are retained.

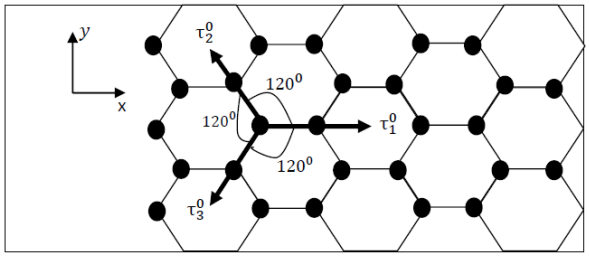

Fig. 5 A Zigzag SWCNT

As mentioned above, a SWCNT is constructed from three doublets having equal lengths and angles between them, an example of which is a Zigzag SWCNT ($\theta = 0$ in Fig. 3) shown in Fig. 5.

Considering Fig. 5, the director vectors in cylindrical coordinates can be expressed as:

$$\tau_{1r}^0 = 0\,, \tau_{2r}^0 = 0\,, \tau_{3r}^0 = 0 \qquad (36)$$

$$\tau_{1\theta}^0 = 0\,, \tau_{2\theta}^0 = -cos30\,, \tau_{3\theta}^0 = cos30 \qquad (37)$$

$$\tau_{1z}^0 = -1\,, \tau_{2z}^0 = -cos60\,, \tau_{3z}^0 = -cos60 \qquad (38)$$

where z is in the axial direction and r and θ are in the radial and circumferential directions of the nanotube, respectively.

If (36) - (38) are substituted into (35), the equation of motion for Zigzag nanotubes are obtained in nonlinear RBM vibration as

$$-\frac{1}{R^2}\frac{E}{1-\nu^2}\left[u_r + \frac{1}{8}\frac{1}{R}u_r^2\right] = \rho\frac{\partial^2 u_r}{\partial t^2} \qquad (39)$$

The above is the expression for the nonlinear RBM frequency of an Armchair SWCNT with scale effects.

The advantage of these simple expressions is that they show the dependency of the RBM frequency on the mechanical and geometrical properties of the SWCNT. In particular, the expressions show that by increasing the Young's modulus (E) and the Poisson's ratio (ν) of the SWCNT, their RBM frequency increases; however by increasing the mass density (ρ), the scale parameter (η) and the radius (r), their RBM frequency decreases.

In the linear condition where $u_r^2 = 0$, from the above equations, it is found that

$$-\frac{1}{R^2}\frac{E}{1-\nu^2}u_r = \rho\frac{\partial^2 u_r}{\partial t^2} \qquad (40)$$

which is in exact agreement with the expression for the linear RBM equation of motion in the scale less condition [9].

4- Application of HPM for solving nonlinear RBM vibrations of SWCNTs

Now, the nonlinear equation of motion is solved to obtain the nonlinear natural frequency in RBM. Assuming $u_r(x,t) = \varphi(x)U(t)$ where $\varphi(x)$ is the eigenmode of the tube satisfying the kinematic boundary conditions and is the time-dependent deflection parameter of the nanotube and applying the Galerkin method, the governing equations of motion are obtained as follows:

$$-\frac{1}{R^2}\frac{E}{1-\nu^2}\left[a_1 U + \frac{1}{8}\frac{1}{R}a_2 U^2\right] = \rho a_1\frac{\partial^2 U}{\partial t^2} \qquad (41)$$

The above equations are the differential equations of motion governing the nonlinear RBM vibrations of CNTs subjected to the following initial conditions:

$$U(0) = U_{max}, \frac{dU}{dt}(0) = 0 \qquad (42)$$

where U_{max} denotes the maximum amplitude of oscillation. In (41), a_1 and a_2 are defined as follows:

$$a_1 = \int_0^L \varphi^2(x)dx\,, a_2 = \int_0^L \varphi^3(x)dx \qquad (43)$$

Under the transformations $r = \sqrt{\frac{I}{A}}$, $\tau = \omega t$, and $w = \frac{U}{r}$, (41) can be transformed to the following nonlinear equation:

$$\omega^2 \frac{d^2W}{\partial\tau^2} + AW + BW^2 = 0 \quad (44)$$

wherein

$$A = \frac{1}{R^2\rho}\frac{E}{1-\nu^2} = \omega_L^2 \quad (45)$$

$$B = \frac{1}{R^2\rho}\frac{E}{1-\nu^2}\sqrt{\frac{I}{A}}\frac{1}{8}\frac{1}{R}\frac{a_2}{a_1} \quad (46)$$

In (45), $\omega_L = \sqrt{A}$ is the linear, free vibration frequency in the RBM. In (44), the unknown angular frequency has to be determined. To this end, HPM is applied to seek the solution of (44). The following homotopy with ω_0 as the initial approximation for the angular frequency is constructed

$$(1-p)\omega_0^2\left(\frac{d^2U}{\partial\tau^2} + AU\right) + p\left(\omega^2\frac{d^2U}{\partial\tau^2} + AU + BU^2\right) = 0 \quad (47)$$

Here p is a parameter, $W = W(\tau, p)$ and $\omega = \omega(p)$. Obviously, when $p = 0$, (47) yields the following linear harmonic equation

$$\frac{d^2W}{\partial\tau^2} + W = 0\,, W(0) = W_{max}\,, \frac{dW(0)}{\partial\tau} = 0 \quad (48)$$

It is notable that for $p = 1$, it results the nonlinear Eq. (44). As embedding parameter p varied from 0 to 1, the solutions $W = W(\tau, p)$ and $\omega = \omega(p)$ of the homotopy (47) change from their initial approximations $W_0(\tau)$ and ω_0 to the required solutions $W(\tau)$ and ω of Eq. (44). Suppose the solution of Eq. (44) to be in the following form:

$$W(\tau) = W_0(\tau) + pW_1(\tau) + \cdots \quad (49)$$

$$\omega = \omega_0 + p\omega_1 + \cdots \quad (50)$$

Substituting the above relations into the (47) and equaling the coefficients of the terms with same powers of p, the following linear differential equations are obtained

$$\begin{aligned} &p^0: \frac{d^2W_0}{\partial\tau^2} + W_0 = 0\,, W_0(0) = 0\,, \frac{dW_0(0)}{\partial\tau} = W_{max} \\ &p^1: \omega_0^2\left(\frac{d^2W_1}{\partial\tau^2} + W_1\right) + \left(\frac{d^2W_0}{\partial\tau^2} + AW_0 + BW_0^2\right) = 0\,, W_1(0) = 0\,, \frac{dW_1(0)}{\partial\tau} = 0 \\ &\quad\vdots \end{aligned} \quad (51)$$

The solution of the initial zeroth approximation is simply obtained by

$$W_0(\tau) = W_{max}cos(\tau) \quad (52)$$

Substituting (52) into the first approximation (51), it is obtained

$$\omega_0^2\left(\frac{d^2W_1}{\partial\tau^2} + W_1\right) + [-\omega_0^2 W_{max}cos(\tau) + AW_{max}cos(\tau) + BW_{max}^2cos^2(\tau)] = 0 \quad (53)$$

Expanding $cos^2(\tau)$ in its first period using Fourier sine series yields

$$cos^2(\tau) \cong \frac{4}{3\pi}sin(\tau) - \frac{28}{15\pi}sin(3\tau) \quad (54)$$

Substituting (54) into (53) and letting the coefficient of $sin(\tau)$ to be zero in order to eliminate the secular terms, it is found that

$$\omega_0 = \sqrt{A - \frac{4}{3\pi}BW_{max}} \quad (55)$$

It was shown that the nonlinear natural frequency in RBM is dependent to many key factors. A fishbone diagram is depicted to

better understanding the effective factors for determining the nonlinear radial frequency. This diagram is given in Fig. 6.

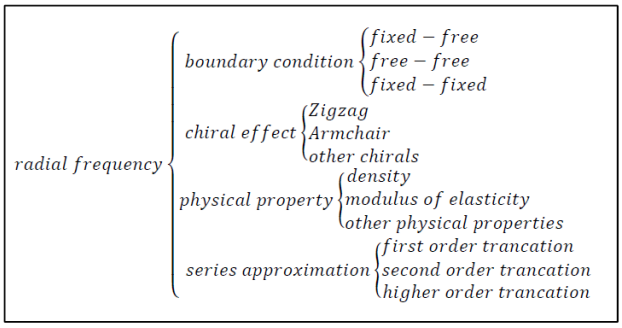

Fig. 6 A fishbone like diagram for effective factors in nonlinear radial frequency

Therefore, the ratio of the nonlinear frequency ($\omega = \omega_0$) to the linear frequency (ω_L) becomes

$$F.R. = \frac{\omega_0}{\omega_L} = \sqrt{1 - \frac{4}{3\pi}\frac{B}{A}W_{max}} \qquad (56)$$

Then, the solution of (53) can be obtained as

$$W_1(t) = -\frac{14}{15}\frac{BW_{max}^2}{3\pi A - 4BW_{max}}[cos(\tau) - cos(3\tau)] \qquad (57)$$

Thus, the first approximate solution of (44) can be written as follows:

$$W(\tau) = W_0(\tau) + W_1(\tau) = W_{max}cos(\tau) - \frac{14}{15}\frac{BW_{max}^2}{3\pi A - 4BW_{max}}[cos(\tau) - cos(3\tau)] \qquad (58)$$

4- Results and discussion

In this section, comparison between the results obtained herein using DM and the available theoretical and experimental results are presented. Throughout this paper, the material properties of SWCNT are taken to be: Young's modulus $E = 1\,TPa$, mass density $\rho = 2300\,\frac{kg}{m^3}$ and Poisson's ratio $\nu = 0.2$ [9, 21]. In the DM model, the scale parameter used is the carbon-carbon bond length $\eta = 0.1421\,nm$ [8].

Table 1: Comparison between RBM frequencies of different Zigzag SWCNTs (cm^{-1}) with different methods.

tube (n, m)	Tube diameter (A^0)	Experimental result [21]	DM result
(6,0)	4.698	475.7	471.3
(7,0)	5.481	407.8	406.4
(8,0)	6.264	356.8	356.1
(9,0)	7.047	317.2	317.5
(10,0)	7.830	285.4	285.9
(11,0)	8.613	259.5	260.1
(12,0)	9.397	237.8	238.8
(13,0)	10.180	219.5	220.1
(14,0)	10.963	203.9	204.7
(15,0)	11.746	190.3	191.1
(16,0)	12.529	178.4	179.0
(17,0)	13.312	167.9	168.7
(18,0)	14.095	158.6	159.0
(19,0)	14.878	150.2	151.2
(20,0)	15.661	142.7	144.1

Table 2: Comparison between RBM frequencies of different Armchair SWCNT (cm^{-1}) with different methods.

tube (n, m)	Tube diameter (A^0)	Experimental result [21]	DM result
(3,3)	4.069	549.3	540.2
(4,4)	5.425	412.0	409.9
(5,5)	6.781	329.6	329.1
(6,6)	8.138	274.6	275.0
(7,7)	9.494	235.4	236.1
(8,8)	10.850	206.0	207.1
(9,9)	12.206	183.1	183.9
(10,10)	13.563	164.8	165.5
(11,11)	14.919	149.8	150.8

In Tables 1 and 2, the radial frequency of different Zigzag and Armchair SWCNTs are shown based on the result presented here along with the available experimental results reported with cm^{-1} [21]. From Tables 1 and 2, we can see that DM predicts the nonlinear radial frequency of different SWCNTs with good agreement with the available experimental result.

Another comparison are done between the results obtained using present method and the available numerical results to validate the presented method. Experimentally, the RBM natural frequency is related to angular frequency ω via $RBM\ f = \frac{w}{2\pi}$.

To demonstrate the accuracy of the obtained analytical results, the variations of nondimensional amplitude vibration are calculated versus nondimensional time for (12, 0) Zigzag tube using present method and numerical method. The numerical method used is fourth-order Runge-Kutta method. From Fig. 7, it can be seen that the result of the present method are in good agreement with the forth-ordered Runge-Kuta numerical results.

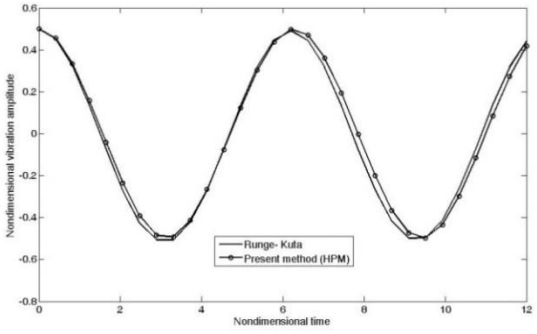

Fig. 7 The nondimensional vibration amplitude of nonlinear RBM (THz) versus nondimensional time for $U_{max} = 0.5$.

Fig. 8 shows the nonlinear natural frequency versus nondimensional amplitude ratio for two Armchair (10, 10) and Zigzag (12, 0) nanotubes. As can be seen from this figure, in contrast to linear systems, the nonlinear frequency is a function of amplitude so that the larger the amplitude, the more pronounced the discrepancy between the linear and nonlinear frequencies becomes. In fact, with increasing the maximum amplitude, the nonlinear frequency decreases. This decreasing is more apparent in higher amplitudes. It should be noted that in the case $B = 0$ the results are in an excellent agreement with those obtained via linear method according to the formulations presented in [9].

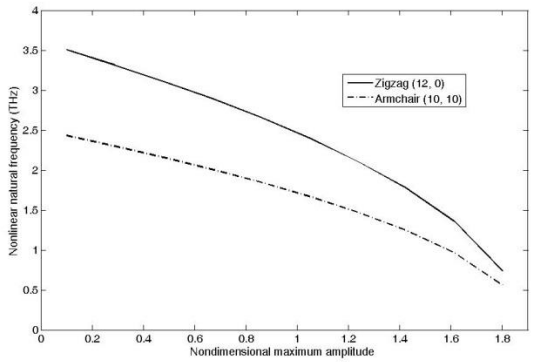

Fig. 8 Nonlinear natural frequency versus nondimensional maximum amplitude of SWNTs for Armchair (10, 10) and Zigzag (12, 0)

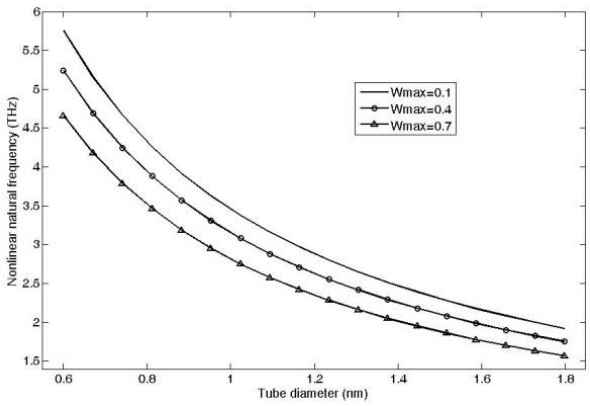

Fig. 9 Variation of nonlinear natural frequency with tube diameter for SWCNTs for different maximum amplitude vibration

Fig. 9 illustrates the nonlinear frequency variation against to diameter of a SWCNT under different maximum amplitude vibrations. It can be observed that with the increase of the tube diameter, the nonlinear vibration frequencies of SWCNTs decrease. This increase is more apparent for lower diameter. As is expected, as the diameter of the tube increaser, the nonlinear frequencies tend to converge to the same value. It is also seen that for the tubes with same diameters, as the maximum amplitude increases, the nonlinear frequencies decreases.

5- Conclusion

In this paper, a detailed investigation of the NRBM frequency of the SWCNT based on DM has been presented. The equation of motion for nonlinear RBM vibration of the SWCNT based on DM is derived. To obtain the nonlinear frequency equation in NRBM vibration, the HPM has been used to investigate the nonlinear vibration analysis of SWCNTs with free end conditions. The significant dependency of this oscillation to tube radius and the amplitude of vibration are observed. The nonlinear vibration frequency of nanotubes rises rapidly with increasing the amplitude especially when the radius of the tube is relatively small. It has been shown that with the increase of the aspect ratio of the nanotubes, the nonlinear vibration frequencies of SWNCTs decrease. It is notable that HPM is straightforward and powerful, and it is a promising technique for solving strong nonlinear partial differential equations like NRBM vibration of SWCNTs. The generated results obtained have been compared with those available in open literature, and excellent correlation has been achieved. The following points are particularly noted. Firstly, the NRBM frequency of vibration of the SWCNT depends on the geometric (radius) and mechanical properties (Young's modulus, density and Poisson's ratio) of the nanotube. Finally, the frequency of the NRBM vibration of the Zigzag SWCNT is slightly higher than that of the Armchair.

References

[1] Fatahi-Vajari, A., & Imam, A. (2016). Lateral Vibrations of Single-Layered Graphene Sheets Using Doublet Mechanics. *Journal of Solid Mechanics*, 8(4), 875-894.

[2] Granik, V.T., & Ferrari, M. (1993). Microstructural mechanics of granular media, *Mechanics of Materials*, 15, 301-322.

[3] Rinaldi, A. & Placidi, L. (2013). A microscale second gradient Approximation of the Damage Parameter of Quasi-Brittle Heterogeneous Lattices, *ZAMM*. 94(10), 862–877.

[4] Forest, S., & Trinh, D. K. (2011). Generalized Continua and Non- Homogeneous Boundary Conditions in Homogenisation Methods, *ZAMM*, 91(2), 90–109.

[5] Eremeyev, V.A., & Lebedev, L.P. (2011). Existence Theorems in the Linear Theory of Micropolar Shells, *ZAMM*. 91(6), 468–476.

[6] Ferretti, M., Madeo, A., Dell'Isola, F., & Boisse, P. (2014). Modeling the onset of shear boundary layers in fibrous composite reinforcements by second-gradient theory, *ZAMP*, 65(3), 587–612

[7] Oveissi, S., Ghassemi, A., Salehi, M., Eftekhari, S. A. & Ziaei-Rad, S. (2023). Analytical determination of non-local parameter value to investigate the axial buckling of nanoshells affected by the passing nanofluids and their velocities considering various modified cylindrical shell theories, *Chinese Physics B*, 32(4), 046201.1-046201.18.

[8] M. Ferrari, V.T. Granik, A. Imam, & J. Nadeau, Advances in Doublet Mechanics (Springer-Verlag, Berlin, 1997

[9] Fatahi-Vajari, A. & Imam, A. (2016). Analysis of radial breathing mode vibration of single-walled carbon nanotubes via doublet mechanics, *ZAMM*. 96(9), 1020-1032.

[10] Xin, J., Zhou, L.X., & Ru, W.J. (2009). Ultrasound attenuation in biological tissue predicted by the modified doublet mechanics model, Chinese Physics Letters, 26(7), 074301.1-074301.4.

[11] Torkan, E., Pirmoradian, M., & Hashemian, M. (2019). Dynamic instability analysis of moderately thick rectangular plates influenced by an orbiting mass based on the first-order shear deformation theory. *Modares Mechanical Engineering*, *19*(9), 2203-2213.

[12] Torkan, E., & Pirmoradian, M. (2019). Efficient higher-order shear deformation theories for instability analysis of plates carrying a mass moving on an elliptical path. *Journal of Solid Mechanics*, *11*(4).

[13] Fatahi-Vajari A., & Imam, A. (2016). Torsional vibration of single-walled carbon nanotubes using doublet mechanics, *ZAMP*. 67(4), 1-22.

[14] Gentile, F., Sakamoto, J., Righetti, R., Decuzzi, P., & Ferrari, M. (2011). A doublet mechanics model for the ultrasound characterization of malignant tissues, *Journal of Biomedical Science and Engineering*. 4, 362-374.

[15] Fang, J.Y., Jue, Z., Jing, F., & Ferrari, M. (2004). Dispersion analysis of wave propagation in cubic-tetrahedral assembly by doublet mechanics, *Chinese Physics Letters*. 21(8),1562-1565.

[16] Fatahi-Vajari A., & Imam, A. (2016). Axial vibration of single-walled carbon nanotubes using doublet mechanics, *Indian Journal of Physics*, 90(4), 447–455.

[17] A. Fatahi-Vajari,: A new method for evaluating the natural frequency in radial breathing like mode vibration of double-walled carbon nanotubes, ZAMM. 10.1002/zamm.201600234

[18] Maultzsch, J., Telg, H., Reich, S., & Thomsen, C. (2005). Radial breathing mode of single-walled carbon nanotubes: Optical transition energies and chiral-index assignment, *Physical Review B*, 72, 205438.1-205438.16.

[19] Basirjafari, S., EsmaeilzadehKhadem, S., & Malekfar, R. (2013). Radial breathing mode frequencies of carbon nanotubes for determination of their diameters, *Current Applied Physics*, 13, 599-609.

[20] Basirjafari, S., EsmaielzadehKhadem, S., & Malekfar, R. (2013). Validation of shell theory for modeling the radial breathing mode of a single-walled carbon nanotube, *IJE TRANSACTIONS A*. 26(4), 447-454.

[21] Bachilo, S. M., Strano, M.S., Kittrell, C., Hauge, R. H., (2002). Smalley, R. E., & Weisman, R. B. Structure-assigned optical spectra of single-walled carbon nanotubes, *Science*, 298, 2361–2366.

[22] He, J. H., (2005). Application of homotopy perturbation method to nonlinear wave equations, *Chaos, Solitons & Fractals*. 26(3), 695–700.

[23] He, J. H. (2006). Homotopy perturbation method for solving boundary value problems, *Physics Letters, Section A*, 350(1-2), 87–88.

[24] J. H. He, Limit cycle and bifurcation of nonlinear problems, Chaos, Solitons & Fractals. 26(3), 827–833 (2005).

[25] He, J. H. (1999). Homotopy perturbation technique, *Computer Methods in Applied Mechanics and Engineering*. 178(3-4), 257–262.

[26] He, J.H. (2005). Homotopy perturbation method for bifurcation of nonlinear problems, *International Journal of Nonlinear Sciences and Numerical Simulation*. 6, 207-208.

[27] He, J. H. (2000). Coupling method of a homotopy technique and a perturbation technique for non-linear problems, *International Journal of Non-Linear Mechanics*, 35(1), 37–43.

[28] He, J. H. (2004). Comparison of homotopy perturbation method and homotopy analysis method, *Applied Mathematics and Computation*, 156(2), 527–539.

[29] He, J. H. (2003). Homotopy perturbation method: a new nonlinear analytical technique, *Applied Mathematics and Computation*, 135(1), 73–79

[30] He, J. H. (2004). The homotopy perturbation method for nonlinear oscillators with discontinuities, *Applied Mathematics and Computation*, 151(1), 287–292.

[31] He, J. H. (2004). Comparison of homotopy perturbation method and homotopy analysis method, *Applied Mathematics and Computation*, 156, 527-539.

[32] He, J. H. (2006). Some asymptotic methods for strongly nonlinear equations, *International Journal of Modern Physics B*, 20(10), 1141–1199.

[33] Ghasemia, M., & Tavassoli Kajani, M. (2010). Application of He's homotopy perturbation method to solve a diffusion-convection problem, *Mathematical Sciences*, **4**(2), 171-186.

[34] Aminikhah, H., & Hemmatnezhad, M. (2011). Nonlinear Vibrations of Multiwalled Carbon Nanotubes under Various Boundary Conditions, *International journal of differential equations*, DOI: 10.1155/2011/343576.

[35] Ghasemi, M., Tavassoli Kajani, M., & Davari, A. (2007). Numerical solution of two dimensional nonlinear differential equation by homotopy perturbation method, *Applied Mathematics and Computation*, 189, 341-345.

[36] Ganji, D. D., (2006). The application of He's homotopy perturbation method to nonlinear equations arising in heat transfer, *Physics Letters*, 355(4-5), 337–341.

[37] Rajabi, A., Ganji, D. D., & Taherian, H. (2007). Application of homotopy perturbation method in nonlinear heat conduction and convection equations, *Physics Letters.* 360(4-5), 570–573.

[38] Abbasbandy, S., (2007). A numerical solution of Blasius equation by Adomian's decomposition method and comparison with homotopy perturbation method, *Chaos, Solitons & Fractals*, 31(1), 257– 260

[39] Biazar J., & Ghazvini, H. (2007). Exact solutions for non-linear Schrodinger equations by He's homotopy perturbation method, *Physics Letters A*, 366(1-2), 79–84.

[40] Cveticanin, L. (2009). Application of homotopy-perturbation to non-linear partial differential equations, *Chaos, Solitons & Fractals*. 40(1), 221–228.

[41] Leung, A. Y. T., & Guo, Z. (2009). Homotopy perturbation for conservative Helmholtz-Duffing oscillators, *Journal of Sound and Vibration*, 325(1-2), 287–296.

[42] Abbasbandy, S. (2006). Numerical solutions of the integral equations: homotopy perturbation method and Adomian's decomposition method, *AppliedMathematics and Computation*, 173(1), 493–500.

[43] Ansari, R., Hemmatnezhad, M., & Ramezannezhad, H. (2010). Application of HPM to the nonlinear vibrations ofmultiwalled carbon nanotubes, *Numerical Methods for Partial Differential Equations*. 26, 490–500.

[44] Rajabi, A. (2007). Homotopy perturbation method for fin efficiency of convective straight fins with temperature dependent thermal conductivity, *Physics Letters A*, 364(1), 33–37.

[45] Raftari, B., & Yildirim, A. (2010). The application of homotopy perturbation method for MHD flows of UCM fluids above porous stretching sheet, Computers & Mathematics with Applications, 59(10), 3328–3337.

Appendix A

Considering scale effects, the relation between the microstrains and displacements up to three terms in the expansion can be written as:

$$\epsilon_\alpha = \frac{1}{2\eta_\alpha^2}\left(\Delta u_{\alpha i}\Delta u_{\alpha i}\tau_{\alpha j}^0\tau_{\alpha j}^0 - \Delta u_{\alpha i}\Delta u_{\alpha j}\tau_{\alpha i}^0\tau_{\alpha j}^0\right) + \frac{\Delta u_{\alpha i}\tau_{\alpha i}^0}{\eta_\alpha}, \Delta \boldsymbol{u}_\alpha = \frac{1}{\eta_\alpha}\boldsymbol{\tau}_\alpha^0.\boldsymbol{\nabla} u_\alpha \qquad \text{(A.1)}$$

The expressions for $\boldsymbol{\nabla}$, $\boldsymbol{\nabla u}$ and $\boldsymbol{\tau}_{\alpha}^{0}$ can be written in the cylindrical coordinates as:

$$\boldsymbol{\nabla}=\begin{bmatrix}\frac{\partial}{\partial r}\\ \frac{1}{r}\frac{\partial}{\partial \theta}\\ \frac{\partial}{\partial z}\end{bmatrix},\boldsymbol{\nabla u}=$$

$$\begin{bmatrix}\frac{\partial u_r}{\partial r} & \frac{1}{r}\left(\frac{\partial u_r}{\partial \theta}-u_\theta\right) & \frac{\partial u_r}{\partial z}\\ \frac{\partial u_\theta}{\partial r} & \frac{1}{r}\left(\frac{\partial u_\theta}{\partial \theta}+u_r\right) & \frac{\partial u_\theta}{\partial z}\\ \frac{\partial u_z}{\partial r} & \frac{1}{r}\frac{\partial u_z}{\partial \theta} & \frac{\partial u_z}{\partial z}\end{bmatrix},\boldsymbol{\tau}_{\alpha}^{0}=\begin{bmatrix}\tau_{\alpha r}^{0}\\ \tau_{\alpha\theta}^{0}\\ \tau_{\alpha z}^{0}\end{bmatrix} \quad (A.2)$$

As a result of the assumptions mentioned in section 3, the gradient operator and the displacement vector are simplified to:

$$\boldsymbol{\nabla}=\frac{\partial}{\partial r}\boldsymbol{e}_r\,,\boldsymbol{u}=u_r(r)\boldsymbol{e}_r \quad (A.3)$$

Then, in the problem considered here, (A.2) are reduced to

$$\boldsymbol{\nabla}=\begin{bmatrix}\frac{\partial}{\partial r}\\ 0\\ 0\end{bmatrix},\boldsymbol{\nabla u}=\begin{bmatrix}\frac{\partial u_r}{\partial r} & 0 & 0\\ 0 & \frac{1}{r}u_r & 0\\ 0 & 0 & 0\end{bmatrix},\boldsymbol{\tau}_{\alpha}^{0}=$$

$$\begin{bmatrix}0\\ \tau_{\alpha\theta}^{0}\\ \tau_{\alpha z}^{0}\end{bmatrix} \quad (A.4)$$

From (A.4), $\boldsymbol{\tau}_{\alpha}^{0}.\boldsymbol{\nabla u}$ can be written as:

$$\boldsymbol{\tau}_{\alpha}^{0}.\boldsymbol{\nabla u}=\begin{bmatrix}0\\ \frac{1}{r}\tau_{\alpha\theta}^{0}u_r\\ 0\end{bmatrix},\boldsymbol{\tau}_{\alpha}^{0}.(\boldsymbol{\tau}_{\alpha}^{0}.\boldsymbol{\nabla u})=$$

$$\frac{1}{r}\left(\tau_{\alpha\theta}^{0}\right)^{2}u_r \quad (A.5)$$

Then, from (A.1), $\Delta\boldsymbol{u}$ is obtained as

$$\Delta\boldsymbol{u}=\begin{bmatrix}0\\ \frac{1}{r}\tau_{\alpha\theta}^{0}u_r\\ 0\end{bmatrix} \quad (A.6)$$

Similarly, the following expressions can be calculated

$$\frac{1}{2\eta_{\alpha}^{2}}(\Delta\boldsymbol{u}.\Delta\boldsymbol{u}\boldsymbol{\tau}_{\alpha}^{0}.\boldsymbol{\tau}_{\alpha}^{0})=\frac{1}{2r^{2}}\left(\tau_{\alpha\theta}^{0}\right)^{2}\left[\left(\tau_{\alpha\theta}^{0}\right)^{2}+(\tau_{\alpha z}^{0})^{2}\right]u_r^{2} \quad (A.7)$$

$$\frac{1}{2\eta_{\alpha}^{2}}(\boldsymbol{\tau}_{\alpha}^{0}.\Delta\boldsymbol{u}\boldsymbol{\tau}_{\alpha}^{0}.\Delta\boldsymbol{u})=\frac{1}{2r^{2}}\left(\tau_{\alpha\theta}^{0}\right)^{4}u_r^{2} \quad (A.8)$$

If (A.6-8) are substituted into (A.1), the following equation for microstrain is obtained

$$\epsilon_{\alpha}=\frac{1}{r}\left(\tau_{\alpha\theta}^{0}\right)^{2}u_r+\frac{1}{2r^{2}}\left(\tau_{\alpha\theta}^{0}\right)^{2}(\tau_{\alpha z}^{0})^{2}u_r^{2} \quad (A.9)$$